In Silico Study of Aluminum Phosphate as Vaccine Adjuvants: Exploring the Binding Interaction of Three Structures of Aluminum Phosphate with Lysozyme and Bovine Serum Albumin

Etik Mardliyati [1,*] , **Damai Ria Setyawati** [1], **Abu Saad Aqueel Ahmad Ansari** [2] , **Muhammad Miftah Jauhar** [2] , **Putri Hawa Syaifie** [2,*]

[1]   Research Center for Vaccine and Drugs, National Research and Innovation Agency (BRIN), Cibinong 16911, Indonesia
[2]   Nano Center Indonesia, Jl. PUSPIPTEK, South Tangerang, Banten, 15314, Indonesia
*   Correspondence: etik002@brin.go.id (E.M.); putri@nano.or.id (P.H.S.);

Abstract: To better understand antigen-aluminum phosphate adjuvant interaction, the binding mechanism of three structures of aluminum phosphate with model proteins (i.e., lysozyme and bovine serum albumin) was explored by in silico calculations. Molecular docking simulations were performed using Autodock tools. A blind docking strategy was utilized to see a conceivable binding mode of aluminum phosphate with the target. Three structures of aluminum phosphate explored were $Al(PO_4)_3$, $AlOH(PO_4)_2$, and $Al(OH)_2PO_4$. Three different PDB structures of each lysozyme and BSA were used to confirm the binding constancy of ligands from different depositors at different resolutions. The results showed that all aluminum molecules bound to the same pocket of lysozyme at a stable conformer, in which hydrogen bonds and salt bridge interactions were dominant in the binding area of ligands. $AlOH(PO_4)_2$ has a better binding mode of interaction with lysozyme than other structures of aluminum phosphate. According to Ramachandran's analysis, the antigen-binding complex with $AlOH(PO_4)_2$ preserves more than 85% of all residues in the favored region. Compared with BSA, $AlOH(PO_4)_2$ poses better binding interactions and binding mode of action to lysozyme with more electrostatic, salt bridge interactions and hydrogen bonds formed.

Keywords: vaccine adjuvant; aluminum phosphate; lysozyme; bovine serum albumin; binding interaction; in silico

1. Introduction

Aluminum-based adjuvant (alum) has been extensively used for a long time in vaccine formulation to stimulate the immune response of poorly immunogenic antigens. Vaccine formulations are basically prepared by adsorption of antigen onto adjuvant. The immune-stimulation effect of alum is mainly associated with the degree of antigen adsorption on the adjuvant. Therefore, it has been generally accepted that antigens should be largely adsorbed by the adjuvant to stimulate an optimal immune response [1].

Vaccine antigen adsorption to alum provides a prolonged release of antigen over time after vaccine administration [2,3]. As a result, alum-adsorbed antigen was more effectively taken up by dendritic cells than soluble antigens, hence enhancing activation of antigen-specific T cells [4–6]. This depot effect is mainly influenced by the physical properties of alum,

including surface area, electric charge, and morphological structure [3]. Antigen adsorption to adjuvant generally occurs by electrostatic, hydrogen bonding, hydrophobic, and covalent or ligand exchange interaction [7]. Electrostatic interaction occurs when the antigen and adjuvant have opposite charges and represent a major mechanism for the adsorption of antigens to alum [6].

The type of alum most commonly used in licensed vaccines is aluminum hydroxide and aluminum phosphate [8]. Aluminum phosphate adjuvant is chemically amorphous aluminum hydroxyphosphate, $Al(OH)_x(PO_4)_y$. It is a nonstoichiometric compound in which the ratio of hydroxyl to phosphate highly depends on the reactants and precipitation conditions [9–11]. The surface charge of a colloidal system is described by the point of zero charge (PZC). The PZC of aluminum phosphate adjuvant depends on the ratio of hydroxyl anion to phosphate anion, which can be decreased by replacing hydroxyl anion with phosphate anion. Commercial aluminum phosphate adjuvant generally has a PZC of 4.6 – 5.6; thus, it has a negative surface charge at neutral pH. Consequently, aluminum phosphate adjuvant is considered to be a good adjuvant candidate for positively charged antigens [11–13].

Since formulating antigen with adjuvant is to get a stable bind between antigen and adjuvant, conditions are generally selected to achieve an optimal binding. Several experimental studies on binding interaction and mechanism of antigen-alum have been investigated [7,14–16]. Nevertheless, information regarding the binding interaction of antigen-adjuvant at a molecular level using high throughput bioinformatic analysis is less reported. In particular, since aluminum phosphate adjuvant has no fixed ratio of hydroxyl to phosphate ion, binding interaction should be highly influenced by the aluminum phosphate structures [17]. Understanding the binding mechanism of antigen-adjuvant at a molecular level will assist in an appropriate design and choice of aluminum phosphate structure that is most suitable for antigen used in vaccine formulation.

The molecular docking approach enables researchers to investigate the biological activity characteristics of compounds at the molecular level. The binding energies, binding site, binding mode, key residues, and types of chemical interactions can be assessed via molecular docking [18–22]. Molecular docking simulation strengthens in vitro assay results by describing how the sample can interact with the targets. The docking result may also reveal the key residues and binding site interaction between aluminum molecules and the protein target. Furthermore, the best aluminum structures might be thoroughly examined when selecting the best ligand structures based on the best mode of interactions [18,23–26].

This study aims to explore the binding interaction of three structures of aluminum phosphate with two model proteins by computational approach. Three structures of aluminum phosphate studied was $Al(PO_4)_3$, $Al(OH)(PO_4)_2$ and $Al(OH)_2(PO_4)$. Lysozyme (LYS) and bovine serum albumin (BSA) were chosen as model protein antigens since they represent proteins' positive charge and negative charge. Herein, molecular docking analysis was accomplished to examine adjuvant's binding mode of action with the specific site of protein at the molecular level.

2. Materials and Methods

2.1. Design of aluminum phosphate structures and their toxicity prediction.

The initial guess structures were generated using Avogadro software. Hartree-Fock calculations were performed using the Orca 5.0 program to optimize the structures. The

geometries were optimized using the 3-21G basis set. The atoms were allowed to relax during optimization. Smiles notations of all aluminum phosphate structures were submitted to PKCSM [27] for rat acute oral toxicity (LD50) prediction and submitted to Protox II for evaluation of their potential hepatotoxicity, carcinogenicity, immunotoxicity, mutagenicity, and cytotoxicity [28].

2.2. Molecular docking simulation.

For modeling the interaction between three structures of aluminum phosphate with lysozyme and bovine serum albumin, molecular docking simulations were performed using Autodock tools 1.5.7 version [29]. A blind docking strategy was utilized to see the conceivable binding mode of aluminum phosphate molecules with the target in the lowest energy. The X-ray crystal structure of lysozyme and BSA were obtained from the Research Collaboratory for Structural Bioinformatics-Protein Data Bank (RCSB-PDB) (https://www.rcsb.org/), using Homo sapiens designated as the source organism. Three different PDB structures of each lysozyme and BSA were used to confirm the binding constancy of ligands from different depositors at different resolutions. For lysozyme, we used protein structure with PDB ID 1HSW, 1DPX, and 2VB1 with resolutions of 2Å, 1.65Å, and 0.65Å, respectively. For BSA, the protein structures with PDB IDs 3V03, 4OR0, and 4F5S were used at resolutions of 2.7Å, 2.58Å and 2.47Å, respectively. All protein structures were prepared using Autodock tools and Biovia Discovery Studio visualizer. First, water molecules and heteroatoms were removed using Biovia discovery and saved in .pdb format. Next, we will add hydrogen polar, merge merging non-polar, and add Kollman charges in Autodock tools, but first, we have to check missing atoms in the structure. Finally, all structures were saved in the pdbqt format after being prepared in Autodock. Aluminum phosphate molecules are also prepared in Autodock tools by adding hydrogen polar, merging non-polar, and adding a gesteiger charge, then saving them in pdbqt format. To start the docking simulation, the grid size of each protein was set to cover the whole structure, which is appropriate for the blind docking method. In PDB ID 1HSW, electrostatic maps were computed using grids of 104, 108, and 118 points in the X, Y, and Z dimensions. PDB ID 1DPX grids of 106, 90, and 100 points in the X, Y, and Z dimensions were used. In PDB ID 2VB1, grids of 88, 104, and 124 points in the X, Y, and Z dimensions were used. Grid spacing of 0.375Å was used for all molecular blind docking simulations, and the center of molecules was used as the coordinate grid center. To predict the binding strength of aluminum phosphate molecules, we ran the genetic algorithm (GA) 50 times with a population size of 150, 2500000 times energy evaluation, maximum generation number of 27000, mutation and crossover rates of 0.02 and 0.8, respectively [19,29–31]**.**

For docking BSA, three different protein structures were used in this study to verify the binding site and energy values. The three crystallized structures were 3V03, 4OR0, and 4F5S. Molecular docking was performed by placing grid boxes with dimensions of $40 \times 40 \times 40$ Å along x, y, and z, respectively, on all BSA structures. The grid centers along the x, y, and z axes were set to 30.680, 27.625, and 43.096 for 3V03; 1,375, 27,254, 107,264 for 4OR0; and 2.166, 28.4945, 107.243 for 4F5S. A grid spacing of 0.375 Å was used for all simulations. The rest of the setup was done the same as for blind docking [32].

Molecular docking results in .dlg format were analyzed in Autodock tools. Out of fifty probable binding sites of aluminum phosphate molecules, only the conformation's lowest binding energy was considered the best pose of docking simulations. The protein-ligand complexes were analyzed in detail utilizing open-source PyMol [33, and the interaction and

distance of the binding site with a protein-ligand interaction profiler (PLIP) [34] were calculated. In order to obtain a comprehensive binding position analysis, the complexes were further visualized in Biovia Discovery Studio [35].

2.4. Ramacandran plot analysis of complex aluminum phosphate-lysozyme and aluminum phosphate-BSA.

The best position of aluminum phosphate to lysozyme and BSA was determined using Autodock tools analysis and saved in pdb format .PDB files of each complex were submitted to SAVES (http://nihserver.mbi.ucla.edu/SAVES), and Ramachandran analysis was plotted using PROCHECK [36].

3. Results and Discussion

Aluminum phosphate adjuvant has a molecular formula of $Al(OH)_x(PO_4)_y$ with aluminum as a centered atom. Aluminum has 13 total electrons with a configuration of 10 electrons placed in the first (1s) and second orbital shell (2s,2p); this only leaves three electrons in the last shell (3s, 3p). So, aluminum has 3 valence electrons [37]. Therefore, three possible structures of aluminum phosphate adjuvant can be constructed as: $Al(OH)_0(PO_4)_3$, $AlOH(PO_4)_2$, and $Al(OH)_2PO_4$. Their 2D structure can be seen in Figure 1.
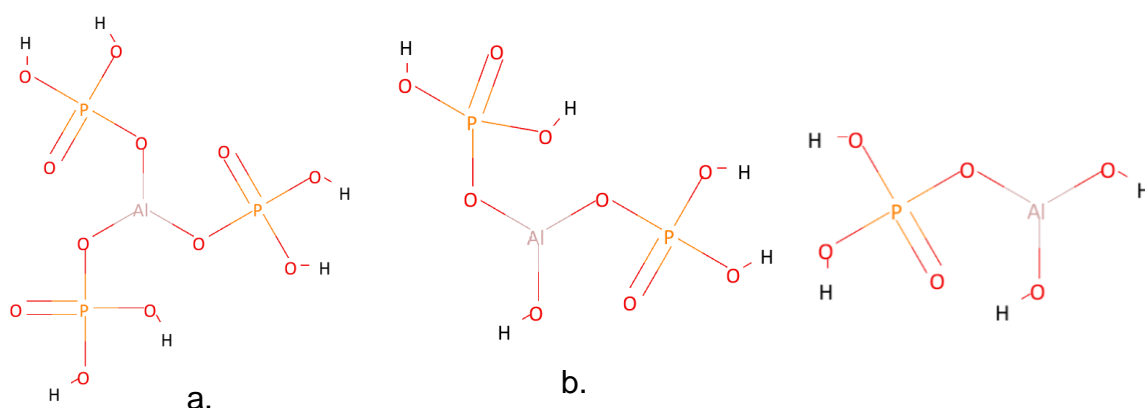

Figure 1. Three forms of aluminum phosphate structures (a) $Al(PO_4)_3$ (b) $Al(OH)_2PO_4$ (c) $AlOH(PO_4)_2$.

Further toxicity prediction of three forms of aluminum phosphate showed that aluminum molecules have less toxicity, and $AlOH(PO_4)_2$ seems saver than other alum molecules, with oral rat acute toxicity (LD_{50}) of 2.081 mol/kg. Toxicity endpoints for all aluminum compounds demonstrate that they are all inactive for hepatotoxicity, carcinogenesis, immunotoxicity, and cytotoxicity. The data is shown in Table 1.

Table 1. Toxicity evaluation of aluminum phosphate structures

Aluminum phosphate structures	LD50 (mol/kg)	Hepatotoxicity	Carcinogenicity	Immunotoxicity	Mutagenicity	Cytotoxicity
$Al(PO_4)_3$	2.015	Inactive	Inactive	Inactive	Inactive	Inactive
$AlOH(PO_4)_2$	2.081	Inactive	Inactive	Inactive	Inactive	Inactive
$Al(OH)_2PO_4$	1.653	Inactive	Inactive	Inactive	Inactive	Inactive

To help a better understanding of how antigens are absorbed by aluminum phosphate adjuvant, molecular docking analysis of the adjuvant with lysozyme or bovine serum albumin (BSA) was further investigated. Lysozyme and BSA have been commonly used as model

antigens in studying antigen uptake and immune response [38–40]. Binding mode of action of the adjuvant to a specific site of protein was investigated in detail.

3.1. Interaction of three forms of aluminum phosphate with lysozyme.

Three forms of aluminum phosphate were investigated for their potential binding to lysozyme by molecular docking. Many crystallized structures of lysozyme are accessible in the RCSB protein database. Therefore, to test the accuracy of the binding energies and validate ligand binding positions, we docked the ligands to three different lysozyme structures and modeled residues. The structures named 1HSW, 1DPX, and 2VB1 have resolutions of 2.0, 1.65, and 0.65 Å, respectively. The grid was constructed to cover the entire lysozyme molecule, allowing aluminum phosphates to move easily to determine the most suitable binding site [41].

Blind docking results are shown in Table 2. The binding energy and inhibition constant of all ligands were varying to all targets. Many factors affect these docking results, including ligand flexibility, residual charge, and structural resolution [42,43]. Only 2VB1 has an ultra-high resolution according to its 0.65 Å structure. Interestingly, the lowest binding energy of all aluminum phosphate ligands was achieved by interaction with 1DPX, while $Al(PO_4)_3$ showed the lowest binding energy of -5.72 kcal/mol. Only the least binding energy result with the most favorable ligand position of 50 docking runs of each ligand was presented in Table 2.

Inhibition constant (Ki) values of docking were in line with binding energy. The higher the negative binding energy values, the lower Ki was observed. Ki represents the inhibitor's affinity for a certain receptor. The lower the Ki value, the less inhibitor is required to limit the reaction rate [44]. All aluminum phosphate molecules show high Ki values to lysozyme. Therefore, these docking results revealed that aluminum phosphate molecules cannot be deemed strong inhibitors compared to the Ki features of a strong inhibitor [45]. This could be because aluminum phosphate molecules not being attached to the active residues in lysozyme, ASP52,nd GLU35 [46,47].

Table 2. Binding energy values of aluminum phosphate with lysozyme.

Aluminum phosphate structures	1HSW		1DPX		2VB1	
	Binding Energy (kcal/mol)	Ki (μM)	Binding Energy (kcal/mol)	Ki (μM)	Binding Energy (kcal/mol)	Ki (μM)
$Al(PO_4)_3$	-3.68	1990	-5.72	64.68	-4.03	1120
$AlOH(PO_4)_2$	-4.06	1050	-5.27	137.28	-5.15	169.16
$Al(OH)_2PO_4$	-4.38	617.69	-5.08	190.09	-4.63	401.86

Figure 2 depicts the docked poses of aluminum phosphate and lysozyme with the lowest energy for each PDB entry of the latter chosen in the current study's important to note that the best conformations of ligands in each PDB structure have the same binding site, and the majority of the amino acids involved in the binding are shared. This result showed that all aluminum phosphate molecules binding to the same pocket of lysozyme at a stable conformer. Current blind docking simulations to different PDB structures showed a valid result according to the same binding pose of all ligands.
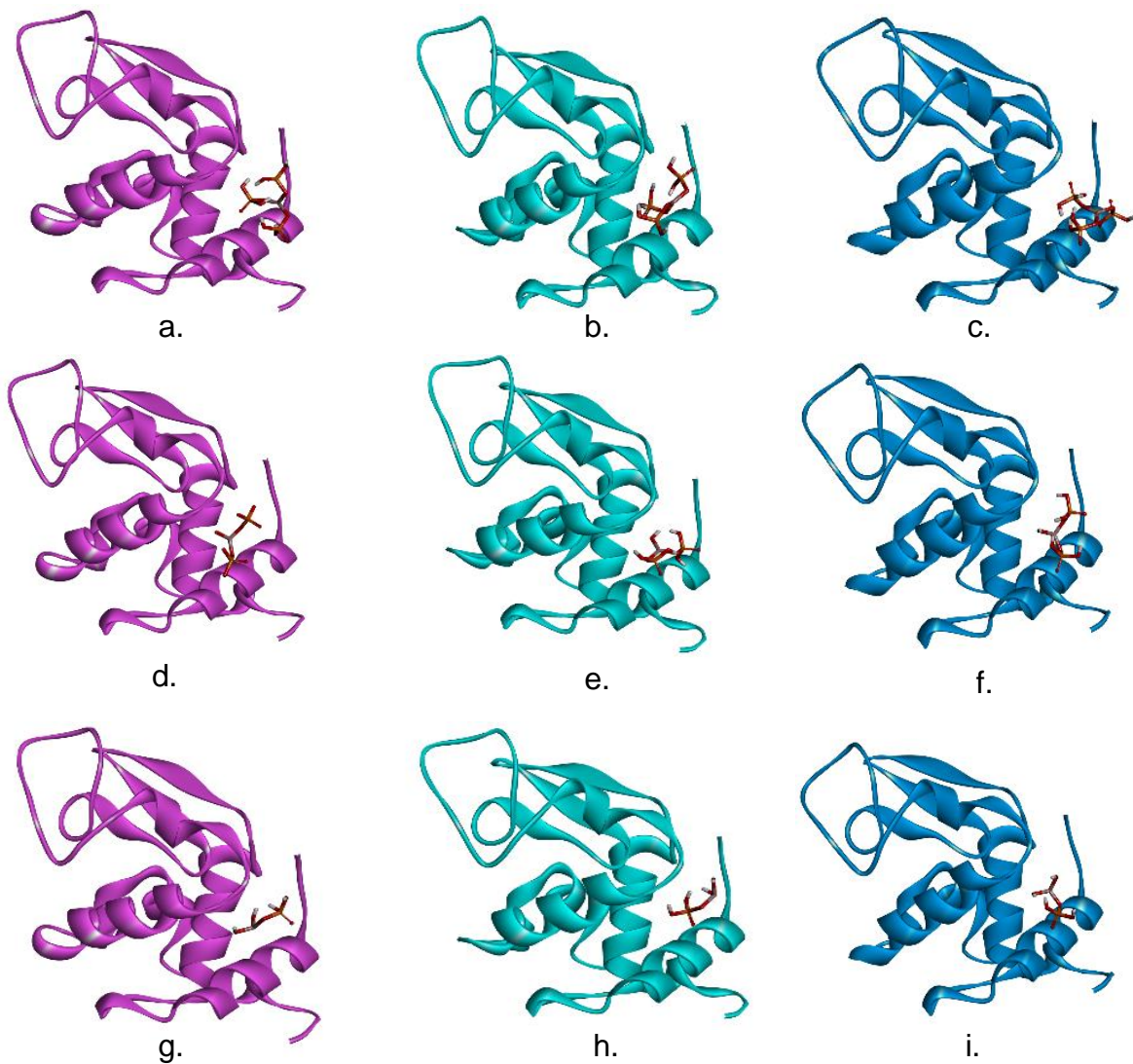
Figure 2. Binding site of aluminum phosphates to different structures of lysozyme, Al(PO$_4$)$_3$ with **(a)** 1HSW **(b)** 1DPX **(c)** 2VB1, AlOH(PO$_4$)$_2$ with **(d)** 1HSW **(e)** 1DPX **(f)** 2VB1, Al(OH)$_2$PO$_4$ with **(g)** 1HSW **(h)** 1DPX **(i)** 2VB1.

Hydrogen bonds and salt bridge interactions were dominant in the binding area of ligands. This is due to the presence of oxygen and phosphorus atoms in ligands. Figure 2 shows that all salt bridge interactions were formed by phosphor atoms in the ligand. Al(PO$_4$)$_3$ has more salt bridge to amino acid residues than Al(OH)$_2$PO$_4$. At least, there were three salt bridge forms in Al(PO$_4$)$_3$ in binding site residues, where this corresponds to the number of P atoms in the ligand. Indeed, one phosphorus atom can form two salt bonds, as illustrated by the AL(OH)(PO$_4$)$_2$ in the binding site of 1HSW.

Figure 3 further demonstrated that oxygen atoms in the PO$_4$ or OH groups typically form hydrogen bonds with the OH or NH atoms of lysozyme amino acid residues. These hydrogen bonds significantly affect the binding energy of ligands to the protein [48] The strength of the hydrogen bonds is affected by the distance between key residues in the protein's active site and the favorable oxygen atoms on the ligand. The stronger the hydrogen bonds, the shorter the distance. Hydrogen bonds with fewer than 3Å are regarded as strong, whereas those with more than 3Å are considered weak [49]. The binding of aluminum phosphate ligands to the active site of lysozyme results in the forming of at least four and up to eight hydrogen bonds. Figure 2E show the most hydrogen bond formed between AlOH(PO$_4$)$_2$ to GLU7,

ARG14, SER86, ASP87, ILE88, and THR89.While, Figure 3a shows the least 4 hydrogens formed between Al(PO4)3 to GLU7, SER86, and ILE88.

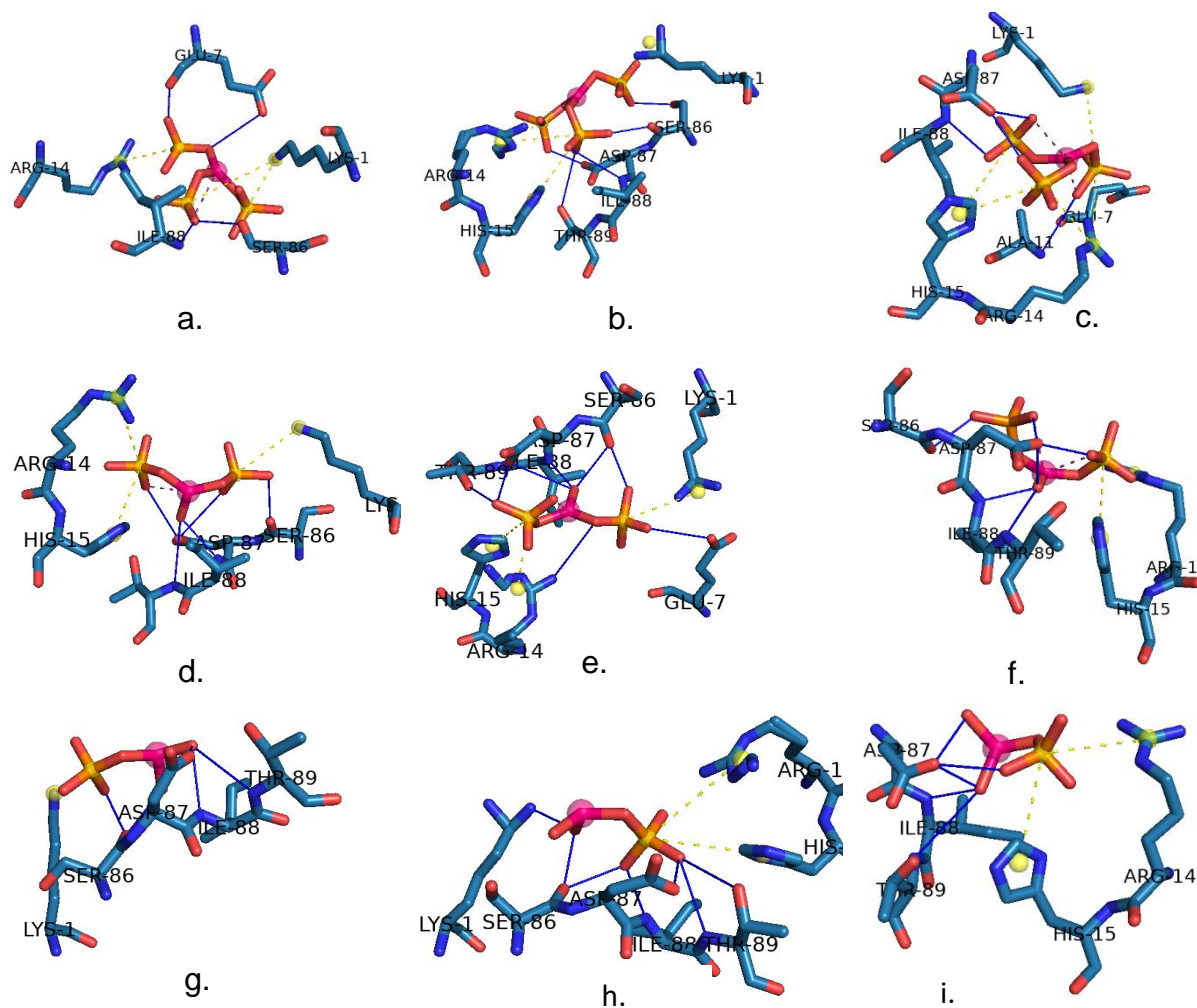**Figure 3.**The interaction of aluminum phosphates in the binding site of lysozyme, Al(PO$_4$)$_3$ with **(a)** 1HSW **(b)** 1DPX **(c)** 2VB1, AlOH(PO$_4$)$_2$ with **(d)** 1HSW **(e)** 1DPX **(f)** 2VB1, Al(OH)$_2$PO$_4$ with **(g)** 1HSW **(h)** 1DPX (i) 2VB1.

LYS1, ARG14, and HIS15 were recognized as important amino acids that form salt bonds with aluminum phosphate molecules at distances ranging from 3 to 5.4Å (Table 3). While GLU7, SER86, ASP87, ILE88, and THR99 mostly form hydrogen bonds with oxygen atoms of ligands at distances ranging from 1.8 to 3.5Å. As mentioned before, Al(PO$_4$)$_3$ shares the least H-bond interaction than AlOH(PO$_4$)$_2$ and Al(OH)$_2$PO$_4$ to the key residues of lysozyme. In the binding site of 1HSW, GLU7, and ILE88 form a strong H-bond to Al(PO$_4$)$_3$ with a distance 1.96Å. while, in 2VB1, strong H bond were formed between ASP87 (distance of 1.82Å) and Al(PO$_4$)$_3$. AlOH(PO$_4$)$_2$ shares more H-bond interaction than other aluminum molecules, especially with 1DPX with eight H bonds in total. Half of the AlOH(PO$_4$)$_2$ H-bonds with 1DPX exhibited strong interactions with a distance of less than 2Å, whereas the shortest H-bond distance depicted to ILE88 is 1.68Å. Interestingly, there were 3 H-bonds formed between AlOH(PO$_4$)$_2$ and ASP87 (observed in the binding site of 1HSW and 2VB1). This is due to the chemical structure of ASP. Aspartic acid has favorable electrophilic and nucleophilic sites of reactions that enable it to be attached by ligand [50]. 3 strong H-bonds with aspartic acid were also observed in the AlOH(PO4)2 to 2VB1 binging site's binding site. Furthermore,

LYS1 was discovered to form a strong H-bond with Al(OH)$_2$PO$_4$ in the 2VB1 binding site, despite LYS1 commonly forming salt bridges with other aluminum phosphate molecules.

Table 3. Analysis of interactions aluminum phosphates in the binding site of lysozyme.

Aluminum phosphate structures	Num.	Residue	1HSW		1DPX		2VB1	
			Bonds	**Distance (Å)**	**Bonds**	**Distance (Å)**	**Bonds**	**Distance (Å)**
Al(PO$_4$)$_3$	1	LYS	2 Salt bridges	5.49 3.08	Salt bridge	4.08	Salt bridge	5.26
	7	GLU	2 H-bond	1.96 3.08	-	-	H-bond	2.07
	14	ARG	Salt bridge	3.95	2 Salt bridges	3.96 4.78	2 Salt bridges	4.16 5.13
	86	SER	H-bond	2.22	2 H-bond	2.21 2.3	-	-
	87	ASP	-	-	H-bond	2.06	2 H-bond	2.21 1.82
	88	ILE	H-bond	1.96	H-bond	3.12	H-bond	2.2
AlOH(PO$_4$)$_2$	1	LYS	Salt bridge	4.15	Salt bridge	4.23	-	-
	7	GLU	-	-	H-bond	3.22	-	-
	14	ARG	Salt bridge	4.52	H-bond	3.37	Salt bridge	4.12
	15	HIS	Salt bridge	3.95	Salt bridge	5.29	Salt bridge	4.37
	86	SER	H-bond	1.83	2 H-bond	2.19 2.21	H-bond	1.88
	87	ASP	3 H-bond	3.29 2.16 3.01	2 H-bond	2.66 3.38	3 H-bond	2.28 1.83 1.92
	88	ILE	H-bond	2.1	H-bond	1.64	H-bond	2.08
	89	THR	H-bond	3.07	H-bond	3.56	H-bond	3.65
AL(OH)$_2$PO$_4$	1	LYS	Salt bridge	4.02	H-bond	1.81	-	-
	14	ARG	-	-	Salt bridge	5.1	Salt bridge	4.22
	15	HIS	-	-	Salt bridge	4.84	Salt bridge	4.4
	86	SER	2 H-bond	2.01 1.92	2 H-bond	2.01 1.91	-	-
	87	ASP	H-bond	1.65	H-bond	1.78	3 H-bond	2.12 1.97 2.11
	88	ILE	H-bond	2.19	H-bond	1.89	H-bond	2.03
	89	THR	H-bond	3.08	2 H-bond	2.94 2.82	H-bond	3.56

As mentioned before, this study showed that AlOH(PO$_4$)$_2$ has a better binding mode of interaction with lysozyme than other forms of aluminum phosphate. It was found that strong hydrogen bonds were formed in the binding of AlOH(PO$_4$)$_2$ to lysozyme (PDB ID: 2VB1). When compared to the interaction of Al(OH)$_2$(PO$_4$) and Al(PO$_4$)$_3$ with lysozyme, their binding energy was not better. The average binding energy of three different structures of lysozyme was -4.48kcal/mol for Al(PO$_4$)$_3$, -4.70 kcal/mol for Al(OH)$_2$PO$_4$, and the lowest binding energy was -4.83 kcal/mol for Al(OH)2PO4. GLU7, ARG14, SER86, ASP87, ILE88, and THR89 were observed as key residues of aluminum binding to lysozyme. Lysozyme is frequently referred to as the first line of defense of innate immunity and s two crucial residues that play an important role in lysozyme activity, namely GLU35 and ASP52. [47,51]. Interestingly, AlOH(PO$_4$)$_2$ did not attach to GLU35 or ASP52, indicating that aluminum phosphate binding did not block lysozyme activity [52]. Ramachandran analysis revealed that more than 85% of the residues in all complex structures of lysozyme-AlOH(PO$_4$)$_2$ are in the most favored region, whereas fewer than 15% are in the additionally allowed zone. Only one lysozyme structure in the 1HSW PDB ID has 0.9% residue in the outlier area, GLN57 (Figure 4).
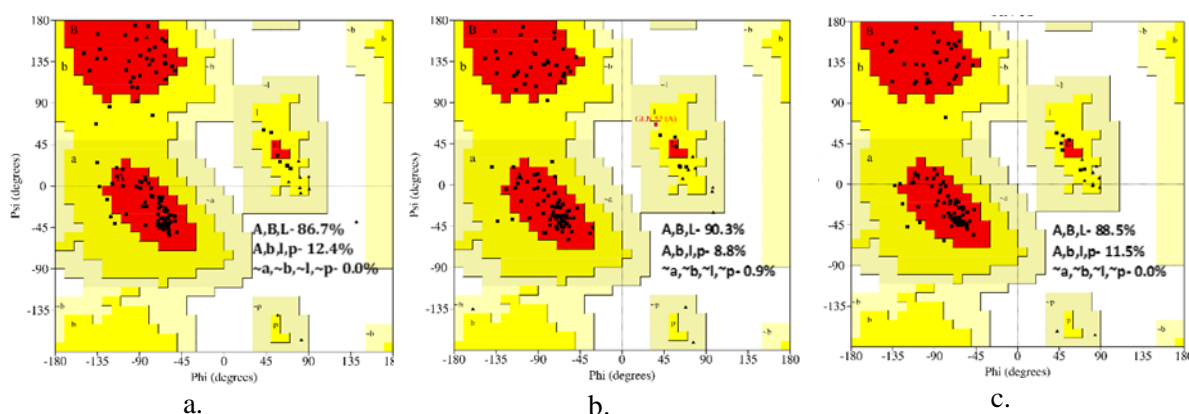
Figure 4. Ramachandran plot analysis of complex AlOH(PO$_4$)$_2$ with lysozyme **(a)** PDB ID: 1HSW **(b)** PDB ID: 1DPX **(c)** PDB ID : 2VB1.

3.2. Interaction of three forms of aluminum phosphate with bovine serum albumin.

Besides lysozyme, bovine serum albumin is often used as a protein model to test the effect of aluminum on immune response via in vitro study.

Despite many BSA structures available in RCSB protein database, the docking of aluminum phosphate molecules was simulated in three different BSA structures to validate the result. BSA proteins used in this study were 3V03, 4OR0, and 4F5S with resolution of 2.7Å, 2.58Å, and 2.47Å, respectively. The BSA structure comprises two chains, A and B, which are heterodimers and have similar numbers of amino acids. These two chains were docked using Autodock tools to assess their molecular contact with aluminum phosphate molecules. BSA Structure consists of three helical domains, which can be divided into two subdomains: IA, IB, IIA, IIB, IIIA, and IIIB. These helical domains account for 74% of all structures, with the rest consisting of two drug sites, drug site 1 placed between the two heterodimers and drug site 2 located in the B chain [53,54]. This docking study focuses on the interaction of Aluminum phosphate with BSA drug site 1.

Table 4. Binding energy values of aluminum phosphate with bovine serum albumin.

Aluminum phosphate structures	3V03		4OR0		4F5S	
	Binding Energy (kcal/mol)	Ki (µM)	Binding Energy (kcal/mol)	Ki (µM)	Binding Energy (kcal/mol)	Ki (µM)
Al(PO$_4$)$_3$	-3.53	2600	-5.08	188.15	-4.54	473.85
AlOH(PO$_4$)$_2$	-5.05	199.62	-5.15	168.8	-4.54	469.41
Al(OH)$_2$PO$_4$	-4.82	291.46	-4.72	344.34	-4.54	473.59

Ligands that docked to 4OR0 showed the lowest binding energy, except for Al(OH)$_2$(PO$_4$). AlOH(PO$_4$)$_2$ with 4OR0 has the lowest binding energy of -5.15 kcal/mol, followed by Al(PO$_4$)$_3$ of -5.08 kcal/mol. These docking results of aluminum ligands to 3V03 and 4OR0 demonstrate the same conclusion that AlOH(PO$_4$)$_2$ has the strongest affinity than other aluminum molecules. They were -5.15 kcal/mol for 4OR0 and 5.05 kcal/mol for 3V03, respectively. Interestingly, all aluminum phosphate molecules share the same binding energy values with 4F5S (-4.54 kcal/mol). These binding values in Table 4 represent the lowest binding energy result with the most favorable ligand location among the 50 docking runs for each ligand.
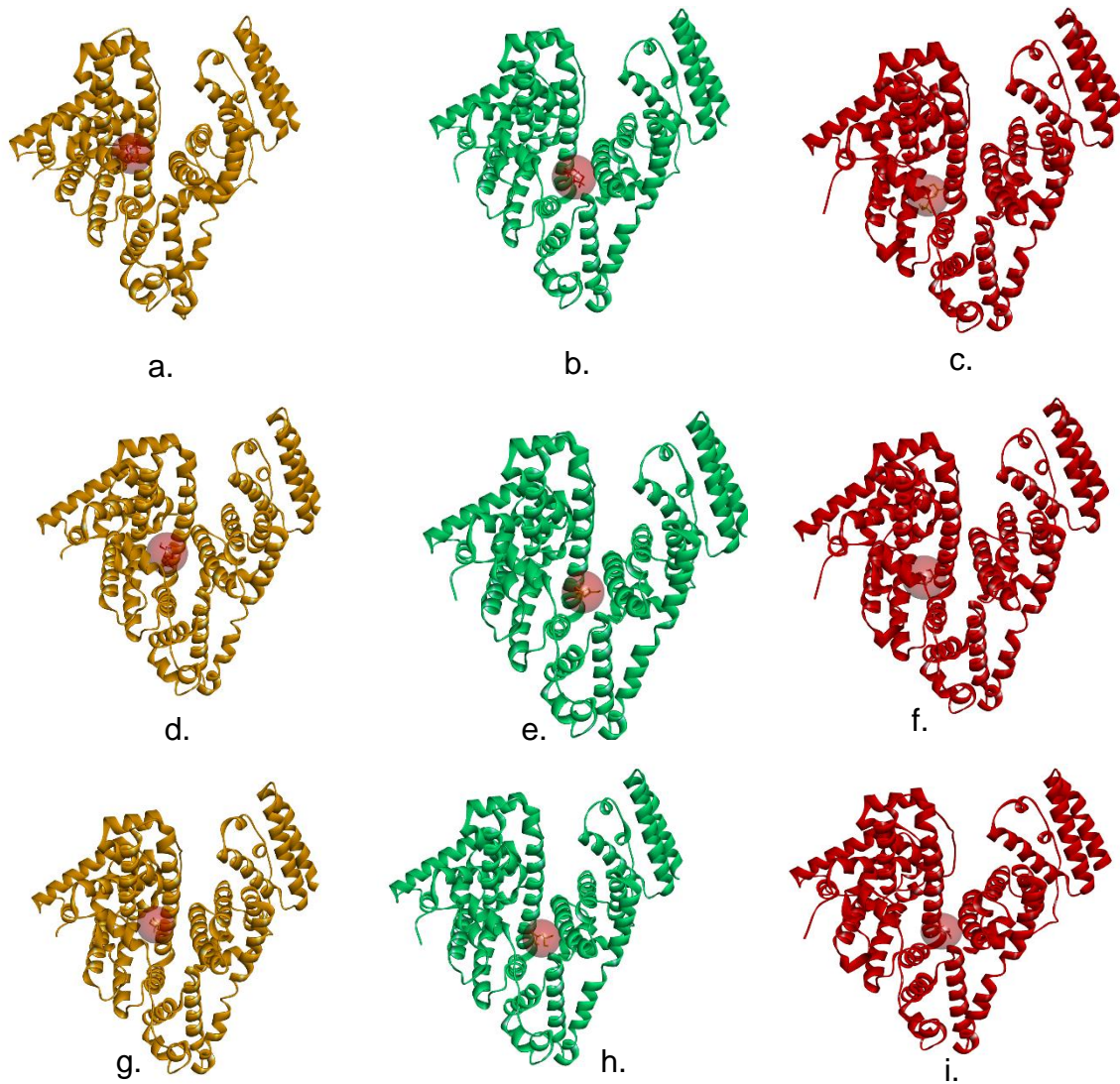
Figure 5. Binding site of aluminum phosphate to different structures of bovine serum albumin, $Al(PO_4)_3$ with **(a)** 3V03 **(b)** 4OR0 **(c)** 4F5S, $AlOH(PO_4)_2$ with **(d)** 3V03 **(e)** 4OR0 **(f)** 4F5S, $Al(OH)_2PO_4$ with **(g)** 3V03 **(h)** 4OR0 **(i)** 4F5S.

Aluminum ligand binding characteristics with BSA are nearly identical to lysozyme, which has a dominant formation of salt bridge interactions and hydrogen bonds. The more phosphorus and oxygen atoms in ligands, the more salt bridge, and hydrogen bonds can be formed. However, the number of interactions created is determined by the docking pose's most stable conformations and lowest binding energy. Each phosphor atom in the ligand can form more than two salt bridge interactions, and each oxygen atom in the ligand can form more than two hydrogen bonds. This could be owing to the distance between the ligand atoms and the active-side residue of BSA [55]. TYR149, SER191, ARG194, ARG198, TRP213, ARG217, GLU291, and ASP450 were observed as active residues in the binding site of aluminum ligands to BSA. These residues can establish salt bridge interactions or hydrogen bonds with phosphorus and oxygen atoms of ligands, respectively.

The salt bridge contact was generated by the contribution of hydrogen bonds and electrostatic forces, resulting in a non-covalent interaction that formed between ionized molecules. This bond is commonly formed by an acid and a base atom with nearby donor-acceptor molecules. As a result, the salt bridge is equivalent to the double charge-assisted hydrogen bond [56]. In the case of salt bridges in aluminum phosphate and BSA complexes,

the proton was transferred from the ligand's phosphate groups, which serve as an acid, to the amine or guanidine side chains of residues, which act as bases. As a result of this proton migration, an H bond and electrostatic contact were formed in the salt bridge in the binding site of the aluminum ligand with BSA. Therefore, in this study, residues with more amine or guanidine groups appear to establish primarily salt bridge interactions with the ligand. Figures 3 and 4 demonstrate that arginine residues 194, 198, and 217 were identified as important residues that created a salt bridge to the ligand. Besides, arginine residues can also generate the H-bond interaction with ligands.
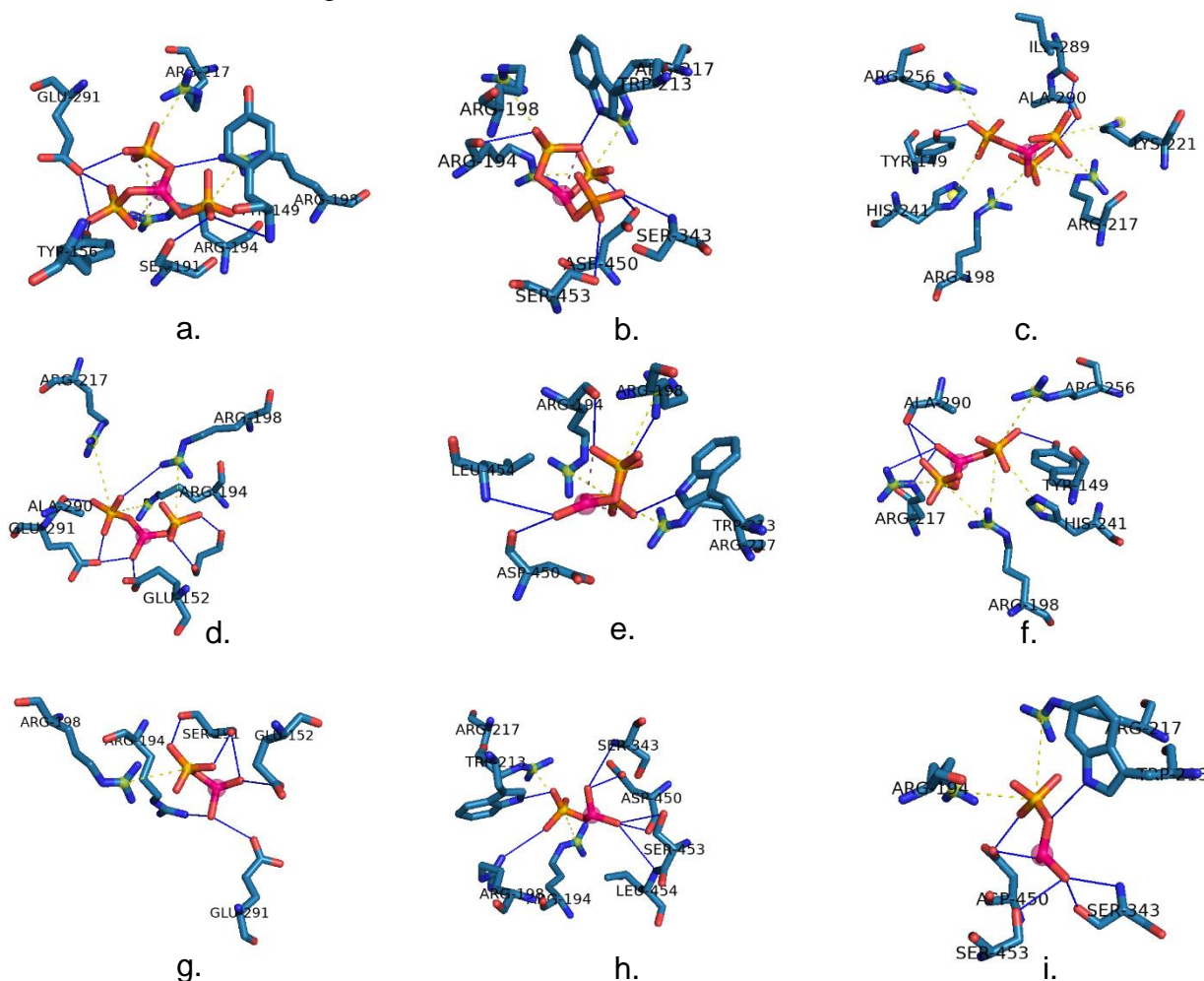

Figure 6. The interactions of aluminum phosphates in the binding sites of bovine serum albumin, Al(PO$_4$)$_3$ with **(a)** 3V03 **(b)** 4OR0 **(c)** 4F5S, AlOH(PO$_4$)$_2$ with **(d)** 3V03 **(e)** 4OR0 **(f)** 4F5S, Al(OH)$_2$PO$_4$ with **(g)** 3V03 **(h)** 4OR0 **(i)** 4F5S.

The interaction analysis of three forms of aluminum phosphate to critical residues of BSA that have the same binding mode is shown in Table 4. In the binding interaction of Al(PO$_4$)$_3$ to 3V03, there were 3 H-bond formed with GLU291, while, in the 4OR0 binding site, 3 H-bond formed with ASP450 to Al(PO$_4$)$_3$. However, in 4F5S, Al(PO$_4$)$_3$ only formed an H-bond to TYR149 with strong interaction (distance 1.64Å). Therefore, the binding energy value of Al(PO$_4$)$_3$ to BSA differed between one another structures (Table. 3). Besides, Al(PO$_4$)$_3$ molecules have a high contribution of torsional free energy to binding energy value; they were +3.58 kcal/mol (data not shown). The formula for binding free energy in Autodock is used to estimate the free energy of binding [57,58].

$$\Delta G_{(\frac{kcal}{mol})} = G\ bound_{(\frac{kcal}{mol})} - G\ unbound_{(\frac{kcal}{mol})}$$

Note :

ΔG = Gibbs energy/ Free binding energy

G bound = Final intermolecular energy + Final torsional energy + Torsional free energy

G unbound = unbound system's energy

Therefore, the higher the free torsional energy, the weaker the ligand binding to the protein's active site. Despite having the same torsional free energy, the binding energy found with $Al(PO_4)_3$ to lysozyme was better than BSA.

$AlOH(PO_4)_2$ and $Al(OH)_2PO_4$ share the same key residues in BSA binding site; they were SER191, ARG194, ARG198, TRP213, ARG217, GLU291, and ASP450, however, only in 4F5S binding site that found TYR149 formed a strong H-bond with $AlOH(PO_4)_2$ (distance 1.93Å). As previously stated, aspartic acid mostly forms salt bridges, while the remaining key residues generate a combination of strong and weak H-bonds depending on their interaction distance. As can be seen in Table 5. $AlOH(PO_4)_2$ binding energy value with BSA was stronger than $Al(OH)_2PO_4$. Despite $AlOH(PO_4)_2$ having higher free torsional energy than $Al(OH)_2PO_4$, they were +2.68 kcal/)2 and +1.79kcal/mol, respectively (data not shown). This condition was the same as the binding of both molecules to lysozyme. However, the binding energy found with $AlOH(PO_4)_2$ to lysozyme was better than BSA.

Table 5. Analysis of interactions aluminum phosphates in the binding site of lysozyme.

Aluminum phosphate structures	Num.	Residue	3V03		4OR0		4F5S	
			Bonds	Distance (Å)	Bonds	Distance (Å)	Bonds	Distance (Å)
AL(PO₄)₃	149	TYR	H-bond	3.28	-	-	H-bond	1.64
	191	SER	H-bond	1.77				
	194	ARG	2 Salt bridge	4.61 5.31	H-bond	2.34	-	-
	198	ARG	H-bond	2.32	Salt bridge	4.68	Salt bridge	3.98
	213	TRP	-	-	H-bond	1.88	-	-
	217	ARG	Salt bridge	5.26	Salt bridge	3.77	2 Salt bridge	5.08 4.52
	291	GLU	3 H-bond	2.18 2.17 2.07	-	-	-	-
	450	ASP	-	-	3 H-bond	3.1 2.48 1.97	-	-
AL(OH)(PO₄)₂	149	TYR	-	-	-	-	H-bond	1.93
	191	SER	2 H-bond	2.24 1.73	-	-	-	-
	194	ARG	Salt bridge	5.2	H-bond	2.13	-	-
	198	ARG	H-bond	3.06	H-bond	3.09	2 Salt bridge	5.27 4.09
	213	TRP	-	-	H-bond	2.2	-	-
	217	ARG	Salt bridge	5.44	-	-	2 H-bond	2.02 3.06
	291	GLU	2 H-bond	1.81 1.83	Salt bridge	3.85	-	-
	450	ASP	-	-	H-bond	3.53	-	-
AL(OH)₂PO₄	191	SER	3 H-bond	1.91 2.01 2.14	-	-	-	-
	194	ARG	H-bond	2.24	Salt bridge	4.22	Salt bridge	4.66
	198	ARG	Salt Bridge	4.35	H-bond	3.22	-	-
	213	TRP	-	-	H-bond	2.18	H-bond	2.17
	217	ARG	-	-	Salt bride	3.8	Salt bridge	5.33
	291	GLU	H-bond	2.13	-	-	-	-
	450	ASP	-	-	2 H-bond	1.83 2.11	2 H-bond	1.91 2.07

This study revealed the same results as docking aluminum to lysozyme that AlOH(PO$_4$)$_2$ showed better interactions with BSA binding sites than other aluminum molecules. As shown in Table 4, AlOH(PO$_4$)$_2$ has the lowest binding energy with different BSA structures than other aluminum molecules, and they are observed to have strong H-bonds and salt bridge interactions. This aluminum binds to drug site 1 of BSA with main residues of ARG194, ARG198, TRP213, and ARG217. These residues are key targets of drugs that strongly bind with BSA. Naproxen, a nonsteroidal anti-inflammatory medicine, was found to form three hydrogen interactions with guanidyl groups of arginines: ARG194, ARG198, and ARG217, as well as one hydrogen bond with the nitrogen group of TRP 213 [54]. 3,5-diiodosalicylic acid, an intermediary for veterinary anthelmintic medicines (closantel and rafoxanide), likewise binds in drug site 1 of BSA via hydrogen bonds to ARG194, ARG198 and ARG217 [53]. Interestingly, Ramachandran's analysis revealed that all BSA- AlOH(PO$_4$)$_2$ complexes contain more than 90% of their residues in the most favored region and none in the outlier area (Figure 7).

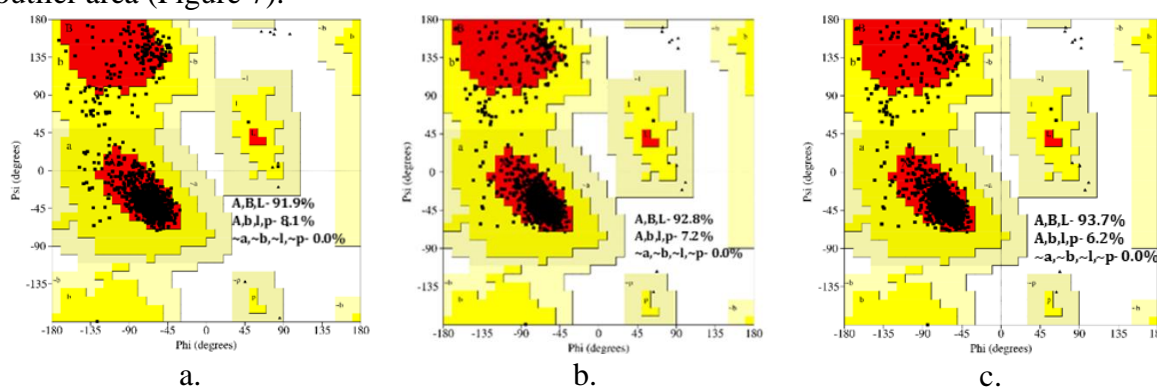**Figure 7.** Ramachandran plot analysis of complex AlOH(PO$_4$)$_2$ with lysozyme **(a)** PDB ID: 3V03, **(b)** PDB ID: 4OR0, **(c)** PDB ID : 4F5S.

Even though aluminum adjuvants have been widely utilized for a long time, it is surprising that the basic formulation characteristics of aluminum adjuvants are sometimes overlooked, and whether aluminum phosphate structures and their interaction with antigens at the molecular level is still unclear. Nevertheless, the antigen-aluminum interaction was essential for researchers to comprehend the molecular basis of this interaction better. The results of this study showed that the interaction of the phosphate group of the alum adjuvant with the side chains of the amine or guanidine residues in the antigen led to the formation of H bond and an electrostatic contact on the surface of the antigen. This interaction, called salt bridges, helps aluminum absorb properly in antigen surfaces. It was consistent with the notion of these molecules' primary surface adsorption, which is influenced by ligand exchange and electrostatic attraction [59,60]. This study also discovered that the hydrogen bonds between the oxygen of alum and the hydroxyl or amine side chain of antigen are crucial in strengthening alum binds with antigen, as determined by their binding energy.

In the role of adsorption of aluminum adjuvants to antigen, aluminum phosphate adjuvants are more attractive to lysozyme antigen than BSA based on their isoelectric points and point of zero charge of aluminum phosphate [6]. This follows the findings of this work, which reveal that the binding of aluminum phosphate to lysozyme resulted in improved interactions based on the low binding energy and the number of interactions created on the lysozyme surface compared to BSA.

4. Conclusions

Based on molecular docking analysis of three structures of aluminum phosphate to lysozyme and BSA, we suggest that a greater ratio of phosphate groups than hydroxyl groups in the aluminum phosphate formula would result in robust binding to the antigen surface. According to Ramachandran plot analysis, the antigen-binding complex with $AlOH(PO_4)_2$ preserves more than 85% of all residues in the favored region. Compared with BSA, aluminum phosphate structures pose better binding interactions and binding modes of action to lysozymes with more electrostatic, salt bridge interactions, and hydrogen bonds formed.

Funding

Acknowledgments

Conflicts of Interest

The authors declare no conflict of interest.

References

1. Huang, M.; Wang, W. Factors affecting alum-protein interactions. *Int. J. Pharm.* **2014**, *466*, 139–146, http://doi.org/10.1016/j.ijpharm.2014.03.015.
2. Kool, M.; Fierens, K.; Lambrecht, B.N. Alum adjuvant: some of the tricks of the oldest adjuvant. *J. Med. Microbiol.* **2012**, *61*, 927–934, http://doi.org/10.1099/jmm.0.038943-0.
3. He, P.; Zou, Y.; Hu, Z. Advances in aluminum hydroxide-based adjuvant research and its mechanism. *Hum. Vaccin. Immunother.* **2015**, *11*, 477–488, http://doi.org/10.1080/21645515.2014.1004026.
4. Sokolovska, A.; Hem, S.L.; HogenEsch, H. Activation of dendritic cells and induction of CD4$^+$ T cell differentiation by aluminum-containing adjuvants. *Vaccine* **2007**, *25*, 4575–4585, http://doi.org/10.1016/j.vaccine.2007.03.045.
5. Awate, S.; Babiuk, L.A.; Mutwiri, G. Mechanisms of action of adjuvants. *Front. Immunol.* **2013**, *4*, http://doi.org/10.3389/fimmu.2013.00114.
6. HogenEsch, H. Mechanism of immunopotentiation and safety of aluminum adjuvants. *Front. Immunol.* **2012**, *3*, http://doi.org/10.3389/fimmu.2012.00406.
7. Callahan, P.M.; Shorter, A.L.; Hem, S.L. The Importance of Surface Charge in the Optimization of Antigen-Adjuvant Interactions. *Pharm. Res.* **1991**, *8*, 851–858, http://doi.org/10.1023/a:1015843210358.
8. Facciolà, A.; Visalli, G.; Laganà, A.; Di Pietro, A. An Overview of Vaccine Adjuvants: Current Evidence and Future Perspectives. *Vaccines* **2022**, *10*, 819, http://doi.org/10.3390/vaccines10050819.
9. Hem, S.L.; HogenEsch, H. Relationship between physical and chemical properties of aluminum-containing adjuvants and immunopotentiation. *Expert Rev. Vaccines* **2007**, *6*, 685–698, http://doi.org/10.1586/14760584.6.5.685.
10. Cerofolini, L.; Giuntini, S.; Ravera, E.; Luchinat, C.; Berti, F.; Fragai, M. Structural characterization of a protein adsorbed on aluminum hydroxide adjuvant in vaccine formulation. *NPJ Vaccines* **2019**, *4*, 20, http://doi.org/10.1038/s41541-019-0115-7.
11. HogenEsch, H.; O'Hagan, D.T.; Fox, C.B. Optimizing the utilization of aluminum adjuvants in vaccines: you might just get what you want. *NPJ Vaccines* **2018**, *3*, 51, http://doi.org/10.1038/s41541-018-0089-x.

12. Rinella, J.V.Jr; White, J.L.; Hem, S.L. Treatment of aluminium hydroxide adjuvant to optimize the adsorption of basic proteins. *Vaccine* **1996**, *14*, 298-300, http://doi.org/ https://doi.org/10.1016/0264-410x(95)00194-6.

13. Burrell, L.S.; Johnston, C.T.; Schulze, D.; Klein, J.; White, J.L.; Hem, S.L. Aluminium phosphate adjuvants prepared by precipitation at constant pH. Part I: composition and structure. *Vaccine* **2000**, *19*, 275–281, http://doi.org/10.1016/s0264-410x(00)00160-2.

14. A1-Shakhshir, R.H.; Regnier, F.E.; White, J.L.; Hem, S.L. Contribution of electrostatic and hydrophobic interactions to the adsorption of proteins by aluminium-containing adjuvants. *Vaccine* **1995**, *13*, 41-44, http://doi.org/10.1016/0264-410x(95)80009-3.

15. Levesque, P.M.; de Alwis, U. Mechanism of Adsorption of Three Recombinant *Streptococcus pneumoniae* (Sp) Vaccine Antigens by an Aluminum Adjuvant. *Hum. Vaccin.* **2005**, *1*, 70–73, http://doi.org/10.4161/hv.1.2.1592.

16. Jully, V.; Mathot, F.; Moniotte, N.; Préat, V.; Lemoine, D. Mechanisms of Antigen Adsorption Onto an Aluminum-Hydroxide Adjuvant Evaluated by High-Throughput Screening. *J. Pharm. Sci.* **2016**, *105*, 1829–1836, http://doi.org/10.1016/j.xphs.2016.03.032.

17. Fox, C.B.; Kramer, R.M.; Barnes L.V.; Dowling, Q.M.; Vedvick, T.S. Working Together: interactions between vaccine antigens and adjuvants. *Ther. Adv. Vaccines* **2013**, *1*, 7–20, http://doi.org/10.1177/2051013613480144.

18. Özbek, D.Ü.; Kuruçay, D. Investigation of In Vitro Effect and Molecular Docking of Aluminum on Glucose-6-Phosphate Dehydrogenase Activity. *Cumhur. Sci. J.* **2022**, *43*, 232–237, http://doi.org/10.17776/csj.1088724.

19. Jauhar, M.M.; Syaifie, P.H.; Arda, A.G.; Ramadhan, D.; Nugroho, D.W.; Kaswati, N.M.N.; Noviyanto, A.; Rochman, N.T.; Mardliyati, E. Evaluation of propolis activity as sucrose-dependent and sucrose-independent *Streptococcus mutans* inhibitors to treat dental caries using an *in silico* approach. *J. Appl. Pharm. Sci.* **2023**, *13,* http://doi.org/10.7324/japs.2023.45365.

20. Syaifie, P.H.; Hemasita, A.W.; Nugroho, D.W.; Mardliyati, E.; Anshori, I. *In Silico* Investigation of Propolis Compounds as Potential Neuroprotective Agent. *Biointerface Res. Appl. Chem.* **2022**, *12*, 8285–8306, http://doi.org/10.33263/BRIAC126.82858306.

21. Harisna, A.H.; Nurdiansyah, R.; Syaifie, P.H.; Nugroho, D.W.; Saputro, K.E.; Firdayani; Prakoso, C.D.; Rochman, N.T.; Maulana, N.N.; Noviyanto, A.; Mardliyati, E. In silico investigation of potential inhibitors to main protease and spike protein of SARS-CoV-2 in propolis. *Biochem. Biophys. Rep.* **2021**, *26*, 100969, http://doi.org/10.1016/j.bbrep.2021.100969.

22. Syaifie, P.H.; Harisna, A.H.; Nasution, M.A.F.; Arda, A.G.; Nugroho, D.W.; Jauhar, M.M.; Mardliyati, E.; Maulana, N.N.; Rochman, N.T.; Noviyanto, A.; Benegas-Luna, A.J.; Pérez-Sánchez, H. Computational Study of Asian Propolis Compounds as Potential Anti-Type 2 Diabetes Mellitus Agents by Using Inverse Virtual Screening with the DIA-DB Web Server, Tanimoto Similarity Analysis, and Molecular Dynamic Simulation. *Molecules* **2022**, *27*, 3972, http://doi.org/10.3390/molecules27133972.

23. Arafat, E.A.; El-Sayed, D.S.; Hussein, H.K.; Flaven-Pouchon, J.; Moussian, B.; El-Samad, L.M.; El Wakil, A.; Hassan, M.A. Entomotherapeutic Role of *Periplaneta americana* Extract in Alleviating Aluminum Oxide Nanoparticles-Induced Testicular Oxidative Impairment in Migratory Locusts (*Locusta migratoria*) as an Ecotoxicological Model. *Antioxid.* **2023**, *12*, 653, http://doi.org/10.3390/antiox12030653.

24. Hamdan, A.M.E.; Alharthi, F.H.J.; Alanazi, A.H.; El-Emam, S.Z.; Zaghlool, S.S.; Metwally, K.; Albalawi, S.A.; Abdu, Y.S.; Mansour, R.E.S.; Salem, H.A.; Elmageed, Z.Y.A.; Abu-Elfotuh, K. Neuroprotective Effects of Phytochemicals against Aluminum Chloride-Induced Alzheimer's Disease through ApoE4/LRP1, Wnt3/β-Catenin/GSK3β, and TLR4/NLRP3 Pathways with Physical and Mental Activities in a Rat Model. *Pharm.* **2022**, *15*, 1008, http://doi.org/10.3390/ph15081008.

25. El-Hawary, S.S.; Sobeh, M.; Badr, W.K.; Abdelfattah, M.A.O.; Ali, Z.Y.; El-Tantawy, M.E.; Rabeh, M.A.; Wink, M. HPLC-PDA-MS/MS profiling of secondary metabolites from Opuntia ficus-indica cladode, peel and fruit pulp extracts and their antioxidant, neuroprotective effect in rats with aluminum chloride induced neurotoxicity. *Saudi J. Biol. Sci.* **2020**, *27*, 2829–2838, http://doi.org/10.1016/j.sjbs.2020.07.003.

26. Liu, S.; Ding, Y.; Yu, Q.; Wang, X.; Cheng, D. Comparative study of aluminum speciation on brain-type creatine kinase: Enzyme kinetic, molecular docking, cellular experiment, and mouse model study. *J. Inorg. Biochem.* **2023**, *238*, 112032, http://doi.org/10.1016/j.jinorgbio.2022.112032.

27. Pires, D.E.V.; Blundell, T.L.; Ascher, D.B. pkCSM: Predicting Small-Molecule Pharmacokinetic and Toxicity Properties Using Graph-Based Signatures. *J. Med. Chem.* **2015**, *58*, 4066–4072, http://doi.org/10.1021/acs.jmedchem.5b00104.

28. Banerjee, P.; Eckert, A.O.; Schrey, A.K.; Preissner, R. ProTox-II: a webserver for the prediction of toxicity of chemicals. *Nucleic Acids Res.* **2018**, *46*, W257–W263, http://doi.org/10.1093/nar/gky318.

29. Huey, R.; Morris, G.M. Using AutoDock with AutoDockTools: A Tutorial in Book The Scripps Research Institute Molecular Graphics Laboratory: California, USA, **2006**;1-51

30. Ali, M.S.; Al-Lohedan, H.A. Spectroscopic and Molecular Docking Investigation on the Non-covalent Interaction of Lysozyme with Saffron Constituent "Safranal." *ACS Omega* **2020**, *5*, 9131–9141, http://doi.org/10.1021/acsomega.9b04291.

31. Huey, R.; Morris, G.M.; Forli, S. Using AutoDock 4 and AutoDock Vina with AutoDockTools: A Tutorial in Book The Scripps Research Institute Molecular Graphics Laboratory **2012**; California, USA, 1-32.

32. Bharathala, S.; Kotarkonda, L.K.; Singh, V.P.; Singh, R.; Sharma, P. *In silico* and experimental studies of bovine serum albumin-encapsulated carbenoxolone nanoparticles with reduced cytotoxicity. *Colloids Surf. B. Biointerfaces* **2021**, *202*, 111670, http://doi.org/10.1016/j.colsurfb.2021.111670.

33. DeLano WL The PyMOL Molecular Graphics System. **2002**.

34. Salentin, S.; Schreiber, S.; Haupt, V.J.; Adasme, M.F.; Schroeder, M. PLIP: fully automated protein-ligand interaction profiler. *Nucleic Acids Res.* **2015**, *43*, W443–W447, http://doi.org/10.1093/nar/gkv315.

35. Biovia, D.S. BIOVIA Discovery Studio Visualizer **2017**, 779.

36. Laskowski, R.A.; MacArthur, M.W.; Moss, D.S.; Thornton, J.M. PROCHECK: a program to check the stereochemical quality of protein structures. *J. Appl. Crystallogr.* **1993**, *26*, 283–291, http://doi.org/10.1107/s0021889892009944.

37. Nakashima, P.N.H.; Smith, A.E.; Etheridge, J.; Muddle, B.C. The Bonding Electron Density in Aluminum. *Science (1979)* **2011**, *331*, 1579–1583, http://doi.org/10.1126/science.1198415.

38. Witeof, A.E.; McClary, W.D.; Rea, L.T.; Yang, Q.; Davis, M.M.; Funke, H.H.; Catalano, C.E.; Randolph, T.W. Atomic-Layer Deposition Processes Applied to Phage λ and a Phage-like Particle Platform Yield Thermostable, Single-Shot Vaccines. *J. Pharm. Sci.* **2022**, *111*, 1354–1362, http://doi.org/10.1016/j.xphs.2022.01.013.

39. Chen, B.; Li, R.; Kubota, A.; Alex, L.; Frangogiannis, N.G. Identification of macrophages in normal and injured mouse tissues using reporter lines and antibodies. *Sci. Rep.* **2022**, *12*, 4542, http://doi.org/10.1038/s41598-022-08278-x.

40. Birchenough, H.L.; Nivia, H.D.R.; Jowitt, T.A. Interaction standards for biophysics: anti-lysozyme nanobodies. *Eur. Biophys. J.* **2021**, *50*, 333–343, http://doi.org/10.1007/s00249-021-01524-6.

41. Ali, M.S.; Waseem, M.; Subbarao, N.; Al-Lohedan, H.A. Dynamic interaction between lysozyme and ceftazidime: Experimental and molecular simulation approaches. *J. Mol. Liq.* **2021**, *328*, 115412, http://doi.org/10.1016/j.molliq.2021.115412.

42. Atkovska, K.; Samsonov, S.A.; Paszkowski-Rogacz, M.; Pisabarro, M.T. Multipose Binding in Molecular Docking. *Int. J. Mol. Sci.* **2014**, *15*, 2622–2645, http://doi.org/10.3390/ijms15022622.

43. Lee, H.S.; Jo, S.; Lim, H.S.; Im, W. Application of Binding Free Energy Calculations to Prediction of Binding Modes and Affinities of MDM2 and MDMX Inhibitors. *J. Chem. Inf. Model.* **2012**, *52*, 1821–1832, http://doi.org/10.1021/ci3000997.

44. Costa, J.d.S.; Ramos, R.d.S.; Costa, K.d.S.L.; Brasil, D.d.S.B.; Silva, C.H.T.d.P.d.; Ferreira, E.F.B.; Borges, R.d.S.; Campos, J.M.; Macêdo, W.J.d.C.; Santos, C.B.R.d An in Silico Study of the Antioxidant Ability for Two Caffeine Analogs Using Molecular Docking and Quantum Chemical Methods. *Molecules* **2018**, *23*, http://doi.org/10.3390/molecules23112801.

45. Türkeş, C.; Demir, Y.; Beydemir, Ş. Infection Medications: Assessment In-Vitro Glutathione S-Transferase Inhibition and Molecular Docking Study. *ChemistrySelect* **2021**, *6*, 11915–11924, http://doi.org/10.1002/slct.202103197.

46. Wang, J.; Dauter, M.; Alkire, R.; Joachimiak, A.; Dauter, Z. Triclinic lysozyme at 0.65 Å resolution. *Acta Cryst. D* **2007**, *63*, 1254–1268, http://doi.org/10.1107/S0907444907054224.

47. Sukumar, N.; Biswal, B.K.; Vijayan, M. Structures of orthorhombic lysozyme grown at basic pH and its low-humidity variant. *Acta Cryst D* **1999**, *55*, 934–937, http://doi.org/10.1107/S0907444998015522.

48. Bork, N.; Du, L.; Reiman, H.; Kurtén, T.; Kjaergaard, H.G. Benchmarking Ab Initio Binding Energies of Hydrogen-Bonded Molecular Clusters Based on FTIR Spectroscopy. *J.Phys. Chem. A* **2014**, *118*, 5316–5322, http://doi.org/10.1021/jp5037537.

49.   Zhang, C.; Ren, Z.; Liu, L.; Yin, Z. Modelling hydrogen bonds in *NN*-dimethylformamide. *Mol. Simul.* **2013**, *39*, 875–881, http://doi.org/10.1080/08927022.2013.775438.

50.   Abdel-Hamid, M.K.; McCluskey, A. *In Silico* Docking, Molecular Dynamics and Binding Energy Insights into the Bolinaquinone-Clathrin Terminal Domain Binding Site. *Molecules* **2014**, *19*, 6609–6622, http://doi.org/10.3390/molecules19056609.

51.   Brott, A.S.; Clarke, A.J. Peptidoglycan O-Acetylation as a Virulence Factor: Its Effect on Lysozyme in the Innate Immune System. *Antibiotics* **2019**, *8*, 94, http://doi.org/10.3390/antibiotics8030094.

52.   Kumari, P.; Kumari, M.; Kashyap, H.K. How Pure and Hydrated Reline Deep Eutectic Solvents Affect the Conformation and Stability of Lysozyme: Insights from Atomistic Molecular Dynamics Simulations. *J. Phys. Chem. B* **2020**, *124*, 11919–11927, http://doi.org/10.1021/acs.jpcb.0c09873.

53.   Majorek, K.A.; Porebski, P.J.; Dayal, A.; Zimmerman, M.D.; Jablonska, K.; Stewart, A.J.; Chruszcz, M.; Minor, W. Structural and immunologic characterization of bovine, horse, and rabbit serum albumins. *Mol. Immunol.* **2012**, *52*, 174–182, http://doi.org/10.1016/j.molimm.2012.05.011.

54.   Bujacz, A.; Zielinski, K.; Sekula, B. Structural studies of bovine, equine, and leporine serum albumin complexes with naproxen. *Proteins: Struct. Funct. Bioinform.* **2014**, *82*, 2199–2208, http://doi.org/10.1002/prot.24583.

55.   Giofrè, S.V.; Napoli, E.; Iraci, N.; Speciale, A.; Cimino, F.; Muscarà, C.; Molonia, M.S.; Ruberto, G.; Saija, A. Interaction of selected terpenoids with two SARS-CoV-2 key therapeutic targets: An *in silico* study through molecular docking and dynamics simulations. *Comput. Biol. Med.* **2021**, *134*, 104538, http://doi.org/10.1016/j.compbiomed.2021.104538.

56.   Kurczab, R.; Śliwa, P.; Rataj, K.; Kafel, R.; Bojarski, A.J. Salt Bridge in Ligand-Protein Complexes - Systematic Theoretical and Statistical Investigations. *J. Chem. Inf. Model.* **2018**, *58*, 2224–2238, http://doi.org/10.1021/acs.jcim.8b00266.

57.   Hill, A.D.; Reilly, P.J. Scoring Functions for Autodock. In Book Glycoinformatics. Methods in Molecular Biology, Lütteke, T., Frank, M., Eds.; Publisher: New York, NY., **2015,** Volume 1273, pp. 467–474, http://doi.org/10.1007/978-1-4939-2343-4_27.

58.   Hall, R.; Dixon, T.; Dickson, A. On Calculating Free Energy Differences Using Ensembles of Transition Paths. *Front. Mol. Biosci.* **2020**, *7*, http://doi.org/10.3389/fmolb.2020.00106.

59.   Peeling, L.; Hentschel, S.; Fox, R.; Hall, H.; Fourney, D.R. Intraoperative spinal cord and nerve root monitoring: a survey of Canadian spine surgeons. *Can.J.Surg.* **2010**, *53*, 324–328.

60.   Hem, S.L.; HogenEsch, H. Relationship between physical and chemical properties of aluminum-containing adjuvants and immunopotentiation. *Expert Rev. Vaccines* **2007**, *6*, 685–698, http://doi.org/10.1586/14760584.6.5.685.